Chevron Folding Patterns and Heteroclinic Orbits

Christopher J. Budd[a], Amine N. Chakhchoukh[a], Timothy J. Dodwell[b,*], Rachel Kuske[c]

[a] *Centre of Nonlinear Mechanics, University of Bath, Claverton Down, Bath, BA2 7AY UK.*
[b] *College of Engineering, Mathematics and Physical Sciences, University of Exeter, Exeter, EX4 4PX, UK.*
[c] *Department of Mathematics, University of British Columbia, Vancouver, BC, Canada, V6T 1Z2*

Abstract

We present a model of multilayer folding in which layers with bending stiffness EI are separated by a very stiff elastic medium of elasticity k_2 and subject to a horizontal load P. By using a dynamical systems analysis of the resulting fourth order equation, we show that as the end shortening per unit length $\mathcal{E}$ is increased, then if k_2 is *large* there is a smooth transition from small amplitude sinusoidal solutions at moderate values of P to larger amplitude chevron folds, with straight limbs separated by regions of high curvature when P is large. The chevron solutions take the form of near heteroclinic connections in the phase-plane. By means of this analysis, values for P and the slope of the limbs are calculated in terms of $\mathcal{E}$ and k_2.

Keywords:
Chevron folding, fourth order equation, heteroclinic connection, bifurcation

1. Introduction

The folding of sedimentary rocks under tectonic compression has historically been of great interest to structural geologists [2, 18, 25], and subject of many different modeling approaches. Aside from the economic implications, due to the correlation between folding and valuable mineral deposits, exposed escarpments of folded rocks often display distinctive patterns. These may be localised or periodic, smooth or non-smooth, regular or chaotic. Examples of this are shown in Fig. 1, and our particular interest in this paper is the zig-zig like chevron folding patterns observed in the second figure. Questions which naturally arise are what mechanisms can produce all types of observed patterns and how can we identify which type of pattern is most likely to form? In this paper we will discuss the nature of these patterns from the perspective of dynamical systems theory, and will derive a model in which we demonstrate that sinusoidal folding patterns are consistent with (low amplitude) periodic orbits arising at bifurcation points whereas non-smooth, chevron-type behaviour, in which we see zig-zag patterns with straight limbs, can be described in terms of near heteroclinic orbits, and that there is a continuous transition between these two types of behaviour.
The focus of the existing modelling work has considered the buckling or folding of a single layered imbedded in a softer matrix [3, 27, 28, 25] and has more recently received much interested from an engineering and mathematical perceptive on localised and sequential folding [19, 23, 6].

*Corresponding Author: t.dodwell@exeter.ac.uk

Much less attention has been given to modelling multilayered folding processes, in part this is due to the inherent analytical difficulties arising from the high nonlinear geometric constraints of layers fitting together. However, these interlayer interactions play a fundamental role in fold pattern selection [28, 25, 11], and understanding this interaction is central to this paper. Biot [4] proposed a continuum model for the deformation of a laminated material under plane stress. In particular he noted that even though the individual layers maybe considered isotropic the layering offers a plane of weakness, giving a natural anisotropy. Biot proposed that the bulk properties of layered materials, could be described by a homogeneous anisotropic (elastic) material, characterised by two constants $G < M$ which describe shear and compressive stiffness respectively. Vertical and horizontal equilibrium equations under plane stress σ, can be combined to a single linear fourth order PDE

$$\left(G - \frac{\sigma}{2}\right) \phi_{xxxx} + (4M - 2G)\, \phi_{xxyy} + \left(G - \frac{\sigma}{2}\right) \phi_{yyyy} = 0, \tag{1}$$

in terms of the *stress function* ϕ. Subject to appropriate boundary conditions, this equation can then be analysed by using the method of characteristics. This equation has a rich variety of solutions. An analysis presented in [4] equates different folded patterns with varying levels of anisotropy ratio G/M. Different levels of anisotropy correspond to different regimes of the fourth order equation (1); at low contrast the system is elliptic, admitting smooth periodic solutions, yet at higher contrast the system becomes hyperbolic leading to (weak) *kink-type* solutions. Whilst the results provide a selection process of different fold types in terms of the anisotropy ratio the results are at odds with both physical intuition and scaled experiments on aggregate materials (e.g. paper); in particular kink-type patterns are readily observed whilst compressing layers of paper under conditions with low anisotropy contrast with $G \sim M$ [32, 20]. Furthermore the two parameters which characterise an anisotropic solid, do not capture the intrinsic length scale of a multilayered material, the layer thickness. The model predicts, in the elliptic range the system buckles into an infinitely small wavelength, which is contradictory with Biot's theory of a dominant wavelength ([3]). The shortcomings of this formulation stem from the assumption that the shear behaviour of a multilayered material can be described by a single parameter (G). In fact the shear parallel to the layers is in general much weaker than the shear stiffness orthogonal layers. For cases in which there are large disparities, models must not only consider the anisotropic nature of shear at the interfaces, but also the individual contributions of layers as they bend (see for example [22, 13, 14]) . In other words, the difference in shear parallel and orthogonal naturally leads to non-symmetry in the shear stresses introducing moments per unit area or *coupled-stresses*. Various contributions have included layer-wise bending mechanics into continuum descriptions of layered media using Cosserat Theory (see for example [22, 1, 14]). This approach regularises the problem, rendering the governing equation fully elliptic and introduces a dominant wavelength into which layers initially buckle. Whilst gradient-enhanced continuum descriptions of layered materials have come some way in addressing the short-comings of Biot's initial model (1), both approaches consider only the onset of folding instabilities and neglect large deformation geometric interactions between layers. These geometric constraints have been investigated by a number of authors for specific mechanics and processes. For example a geometric model for chevron folds is given in [29], kink banding in layered media is described in [32], the formation of parasitic or accommodation structures is studied in [16, 30, 12] and the formation of hinges and delamination at folding induced singularities outlined in [5, 10]. Whilst these approaches give good explanations for the role geometry places in the forming of specific folding scenarios, they each make certain *a-priori* assumptions of the geometry and structure of

the folding patterns.

In this paper, in contrast, we present a simplified nonlinear energy-based model of a periodic multi-layered material. This model will allow us to investigate the role that the constraints of the multilayer geometry play in fold pattern selection, when long layers of rock are buckled from an initially flat state. The model considers a periodic multilayered material of (long) undeformed length $2L$ described by a horizontal variable $x \in [-L, L]$. The material comprises long single elastic layers lying on top of each other with, up to translation, identical displacements $u(x,t) + nh$ where $n = 0, 1, 2, \ldots$ and h is a constant layer separation. These layers are in turn separated by a stiff elastic medium of stiffness k_2, and the whole structure embedded in an elastic material of stiffness k_1. The limit of large k_2 corresponds to the layers lying in close contact so that their patterns of folding are constrained directly by their geometry. We assume that the system is initially lying flat, and then that the layers are compressed horizontally (for example by the action of tectonic motion) and are thus subjected a prescribed end-shortening distance $\Delta(t)$ associated with an (unknown) horizontal axial load $P(t)$. In doing so the layers buckle, compressing and stretching the interlayer material. Initially the layers will deform into small amplitude periodic sinusoidal folds for which the wavelength and the associated buckling axial load P_C, are determined by the elastic constant k_1 [2] and the amplitude by Δ. As the end-shortening Δ and axial load P increase, then for large values of k_2 the layers interact through the elastic medium separating them giving a geometrical constraint to their motion. This in turn leads to more complex folding patterns. In this paper we investigate the folding patterns observed in this case . We will show that when Δ and P are relatively *small* then the buckling patterns are sinusoidal. However, if k_2 is large, so that the two layers interact strongly, then as Δ increases and P also becomes *large*, so that $P = O(k_2)$ we will show that the buckling patterns become chevron in form. Thus this model describes in one system, two of the main folding patterns observed in practice.

The layout of this paper is as follows. In Section 2 we construct a potential energy functional $\mathcal{W}(u)$ for the system. This combines the work done in bending U_B, into a surrounding foundation U_F and stretching the interlayer material U_V as well as work done by the load $P\Delta$ in producing the desired end-shortening. The potential energy functional per unit length is then given by

$$\mathcal{W} = \frac{1}{2L}\int W\,dx \equiv \frac{1}{2L}\int_{-L}^{L} \frac{EIu_{xx}^2}{(1+u_x^2)^{5/2}} + \frac{1}{2}k_1u^2 + \frac{1}{2}k_2h^2\left(1 - \frac{1}{\sqrt{1+u_x^2}}\right)^2 - P\left(\sqrt{1+u_x^2} - 1\right)\,dx. \tag{2}$$

The resulting folding patterns profiles are given by finding the stable stationary functions of the energy W, over all suitably regular functions u which satisfy the end-shortening constraint. In this paper we will concentrate on studying those solution which are periodic in x. These are in turn solutions of the Euler-Lagrange equation

$$\frac{\delta W}{\delta u} \equiv \frac{\partial W}{\partial u} - \frac{d}{dx}\left(\frac{\partial W}{\partial u_x}\right) + \frac{d^2}{dx^2}\left(\frac{\partial W}{\partial u_{xx}}\right) = 0, \tag{3}$$

subject to the end-shortening constraint. In particular they can be regarded as limits of the solutions of the time dependent fourth order parabolic PDE (of Swift-Hohenberg type) which takes the form

$$\frac{\partial u}{\partial t} = -\frac{\delta W}{\delta u} \tag{4}$$

with the constraint that the end-shortening per unit length (i.e *axial strain*) is given by $\mathcal{E}$.

In Section 3 we give a multiscale analysis of the initiation of the folding patterns of (3) when the end-shortening per unit length (the axial strain) $\mathcal{E}$ is small. By using a carefully scaled amplitude equation will show how the axial load P_C and period ℓ_C of the periodic solutions are selected in this case. We shall find that there is a critical value of $k_2h^2 = k^*$ where the solution structure at the bifurcation changes from sub-critical if $k_2h^2 < k^*$ to super-critical when $k_2h^2 > k^*$. In Section 4 a global analysis of the system is presented and in particular we look at the solutions when the axial load P is large, with $P = O(k_2)$. By applying a rescaling and balance argument combined with a phase-plane analysis of the full system, we deduce the existence of chevron folding type structures in the limit of large k_2 and P. These solutions manifest as near heteroclinic connections in the (u_x, u_{xx}) phase-plane, connecting two flat solutions of the form $(u_x, u_{xx}) = (\pm v^*, 0)$ separated in the horizontal by regions of high curvature of width proportional to $1/\sqrt{P}$. In this limit we observe a trade off between work done in bending U_B and the stretching of the interlayer materials U_V. In Section 5 we then translate this analysis into the original physical coordinates and calculate the associated wavelength ℓ and load P in terms of the end shortening per unit length $\mathcal{E}$. In Section 6 these results are then compared to some numerical calculations of both the fold initiation and of its development into full chevron folds. Finally, in Section 7, we give some conclusions and suggestions for further work.

The main results of Sections 3–5 are summarised as follows

Theorem 1
(i) As the axial strain $\mathcal{E}$ increases from zero, we observe small amplitude *sinusoidal-type solutions of (3), with integer wave number n, at the critical axial load of*

$$P = P_C = \sqrt{8EIk_1}$$

with period $\ell_L = L/(n\pi)$ *as close as possible close to*

$$\ell_C = 2\pi\left(\frac{2EI}{k_1}\right)^{1/4}.$$

When $\mathcal{E}$ is small *the period remains pinned at the value ℓ_L and P increases* linearly *so that*

$$P = P_C + \alpha\mathcal{E} + O(\mathcal{E}^2),$$

where the value of α will be given explicitly and is positive for larger values of k_2 and negative for smaller values.

(ii) If k_2 and P are large*, then as $\mathcal{E}$ increase, there are solutions of (3) which for large axial load P have chevron form with straight limbs in which, for most of the interval $x \in [0, \ell]$, the value of $|u'|$ is constant, with*

$$|u'| = \sqrt{\frac{1}{(1-\mathcal{E})^2} - 1}.$$

The limbs are separated by small regions of high curvature of width $O(1/\sqrt{P})$. These solutions have length $\ell = \ell_C(1-\mathcal{E})$, and occur at a load value of

$$P = k_2h^2\left[(1-\mathcal{E})^2 - (1-\mathcal{E})^3\right].$$

(iii) The axial load takes a maximum value of $P = 4k_2h^2/27$ when $\mathcal{E} = 1/3$.

2. The Model and Energy formulation

To construct a model for multi-layer deformation we consider a representative part of the periodic multilayered material described in the introduction in which the identical layers are separated by a vertical distance h. To do this we consider a structure of two long thin linear elastic layers, separated by a linear elastic filling material. We presume that these layers are then part of a much larger periodic structure, which is ultimately embedded in a linear elastic Winkler type foundation. This is presented in Figure 2. In a vertically periodic case we presume that both layers are defined by *identical copies* of their centre-lines, where the upper layer is calculated by translating the lower layer vertically upwards a distance h. Here h defines the natural normal separation of the layers in the undeformed state. Throughout this work a 2-dimensional setting is assumed, where both layers characterised by the fixed horizontal coordinate x and the angle $\theta = \theta(x)$ with the horizontal. The bottom layer is defined by the vertical displacement $u(x)$, and the top layer a translation of this, with displacement $u(x) + h$. We will consider a long layer of rock of length $2L \gg 1$ which is compressed by a horizontal load P to give a total end-shortening $\Delta = 2L\mathcal{E}$, where $\mathcal{E}$ is the end-shortening per unit length or axial strain.

2.1. The total potential energy functional

A convenient way to determine the folding profile is to use an energy formulation. As the layer shortens a distance $\Delta = 2\mathcal{E}L$ under the action of the load P the work done on the system $P\Delta$ is shared between work done in bending each layer (U_B), against the foundation (U_F) and by compressing or stretching the elastic filling material (U_V) between the two layers.

2.1.1. Bending energy, U_B

Classic bending theory [31, pp. 28] gives the bending over a small segment of a beam ds as $dU_B = \frac{1}{2}EI\kappa\, ds$, where κ is the curvature of the beam and EI is the bending stiffness of a single layer. Integrating over the total length of the material, gives the bending energy of both layers per unit length as

$$U_B = \frac{EI}{2L}\int_{-L}^{L}\kappa^2\, ds = \frac{EI}{2L}\int_{-L}^{L}\frac{u_{xx}^2(x)}{(1+u_x^2(x))^3}\frac{ds}{dx}\, dx = \frac{EI}{2L}\int_{-L}^{L}\frac{u_{xx}^2(x)}{(1+u_x^2(x))^{5/2}}\, dx. \tag{5}$$

The quadratic dependence on u_{xx} implies that a sharp corner has very large bending energy, we therefore assume that u has square integrable second derivatives, so that it has a locally bounded bending energy. We observe that chevron folds are likely to have very large second derivatives.

2.1.2. Foundation energy, U_F

In deformation, the layers compress the surrounding foundation and do work against it. We will make the assumption that this foundation is a linear elastic Winkler foundation with elastic modulus k_1. Therefore the work done per unit length into the foundation due to a deflection $u(x)$ is given by

$$U_F = \frac{1}{4L}k_1\int_{-L}^{L}u^2(x)\, dx \tag{6}$$

More complex nonlinear elastic foundation models can be used, and have been extensively investigated in the engineering and mathematical literature ([19], [23]) and give rise to a plethora of complex behaviour. Here however, we investigate the influence of the geometric nonlinearity in the folding process and the role of this in fold selection through a heteroclinic connection. To distill this behaviour we therefore consider only a linear elastic foundation.

2.1.3. The geometric constraint, U_V

The novel feature of this paper, which distinguishes this model from earlier analysis, is the inclusion of the elastic material of modulus k_2 between the two stiff layers. If k_2 is *small* then each of the layers will not feel the influence of the other and the system will behave as a single layered material. However, if k_2 is *large* then the inclusion of the filling material means that each of the layers will feel the effects of the other's deformation. This is crucial to our analysis. In the initial state we will assume that the two stiff layers are perfectly horizontal, and that the elastic layer fills the rectangular region of height h between them. As the stiff layers deform, so this elastic layer is either stretched or compressed. We will assume that the elastic layer is free to slide along the stiff layers. We now give a leading order calculation of the energy stored in compressing or stretching this elastic filling material away from the natural normal separation. The vertical separation between the two layers at the point x is given by h and the angle of the tangent at x is given by $\theta(x)$. Therefore for a given x a first order approximation of the normal separation between layers is given by

$$n = h\cos\theta(x) = \frac{h}{\sqrt{1+u_x^2}}.$$

The total work per unit length U_V, done in compressing this layer from an initial separation of h is then given by

$$U_V = \frac{1}{4L}k_2h^2\int_{-L}^{L}(1-\cos(\theta))^2\,dx.$$

We note that for a parallel folding, where normal separation is constant, and the rock layers are not vertically periodic, then $U_V = 0$.

2.1.4. Work done by the load

We define the shortening of each layer Δ as the amount the end points approach each other due to the deformation $u(x)$

$$\Delta = \int_{-L}^{L}(1-\cos(\theta(s))\,ds = \int_{-L+\Delta/2}^{L-\Delta/2}\sqrt{1+u_x^2}-1\,dx \approx \int_{-L}^{L}\frac{u_x^2}{2}\,dx \tag{7}$$

where s is the arc-length. This end shortening is achieved by the axial load P acting on each layer therefore the total work done on the system is $P\Delta$. There is an important engineering distinction between two forms of loading *dead* and *rigid*. In the dead loading, P is the controlled parameter and the end shortening 2Δ is the measured quantity. In rigid loading it is the other way round with Δ given and P to be determined. Whilst both share the same equilibrium states, their stability are generally different. For geological applications, *rigid* loading is more relevant, since the motion of plates under tectonic action, causes a slow but constant shortening to rock systems, and we will consider this form of loading in this paper.

2.2. Energy formulation

The total strain energy per unit length for the system is the sum of each contributing term seen in the previous section. It is thus given by,

$$\mathcal{W}(x,u) = \frac{1}{2L}\int_{-L}^{L}W(x,u,u_x,u_{xx})\,dx, \tag{8}$$

where

$$W = \frac{EIu_{xx}^2}{(1+u_x^2)^{5/2}} + \frac{1}{2}k_1u^2 + \frac{1}{2}k_2h^2\left(1 - \frac{1}{\sqrt{1+u_x^2}}\right)^2 - P\left(\sqrt{1+u_x^2(x)} - 1\right). \tag{9}$$

The natural space on which to define $\mathcal{W}$ is $H^2_{\text{loc}}(\mathbb{R})$, the space of all functions with second derivatives in $L^2(K)$ for any compact set $K \subset \mathbb{R}$. Finiteness of the first term (bending energy) requires (at least) $u \in H^2_{\text{loc}}(\mathbb{R})$, and this condition naturally insures all other terms are well defined. To consider repeating folding patterns, we augment W with the periodic boundary conditions

$$u(0) = u(\ell), \quad u_x(0) = u_x(\ell), \quad u_{xx}(0) = u_{xx}(\ell) \quad \text{and} \quad u_{xxx}(0) = u_{xxx}(\ell). \tag{10}$$

Here the period $\ell = 2\pi/\omega$ is to be determined. Once known, we can seek periodic solutions over the finite domain $(0, \ell)$.
The application of the axial strain $\mathcal{E}$ implies that if we consider a solution in the interval $s \in [-L, L]$ to be shortened by an amount $2\mathcal{E}L$ then

$$\int_{-L(1-\mathcal{E})}^{L(1-\mathcal{E})} \sqrt{1+u_x^2}\, dx = 2L. \tag{11}$$

2.3. The governing equations

To derive the governing equations for the system we consider the fourth order gradient flow given by

$$\frac{\partial u}{\partial t} = -\frac{\delta W}{\delta u} = -\frac{\partial W}{\partial u} + \frac{d}{dx}\left(\frac{\partial W}{\partial u_x}\right) - \frac{d^2}{dx^2}\left(\frac{\partial W}{\partial u_{xx}}\right). \tag{12}$$

with the constraint that the end-shortening per unit length is given by $\mathcal{E}$. Along this flow it is immediate that

$$\frac{d\mathcal{W}}{dt} = -\int_{-L}^{L}\left(\frac{\delta W}{\delta u}\right)^2 dx < 0. \tag{13}$$

Hence we will seek stationary values of (12) which are in turn minimisers of the total energy $\mathcal{W}$. In our analysis we will firstly look at solutions of small amplitude which arise for small $\mathcal{E}$. We then consider how these solutions evolve as the axial strain $\mathcal{E}$ increases.

3. Fold initiation

3.1. Overview and reduced equation

To start our study, we consider a layer of rock of length $2L \gg 1$ (assumed large compared with the wavelength of any fold) compressed to have an axial strain of $\mathcal{E} = \Delta/2L$ at an (a-priori unknown) axial load P. When the axial strain is zero, the Euler-Lagrange equation (16) has the trivial solution $u(x) = 0$. As the end shortening increases, non-zero sinusoidal periodic solutions of frequency ω and period $\ell = 2\pi/\omega$ occur for certain critical values of the load $P = P_C$ and their amplitude increases in proportion to $\sqrt{\mathcal{E}}$. In this section we will determine these critical values of P and calculate the associated wavelength and amplitude of the solution as functions of $\mathcal{E}$, showing that for small deviations $\omega = \omega_C$ and does not vary, wheras P depends linearly upon $\mathcal{E}$. We will also show that the nature of the bifurcation depends upon the value of k_2. If k_2

is sufficiently large, then as $\mathcal{E}$ increases so the amplitude of the soution and P increases and we will consider the limit of large P in the next section.

Our initial analysis will make the assumption that u and $|u_x(x)|$ are small. This allows us to study the deviation of the system from an initially undeformed state using a stabilty analysis associated with an amplitude equation, we therefore consider the weakly nonlinear Lagrangian, achieved by truncating terms at order u_x^4 given by

$$W = EIu_{xx}^2\left(1 - \frac{5}{2}u_x^2\right) + \frac{1}{2}k_1u^2 + \frac{1}{8}k_2h^2u_x^4 - P\left(\frac{1}{2}u_x^2 - \frac{1}{8}u_x^4\right)\,dx. \tag{14}$$

At the same order of approximation, the end-shortening condition resulting from the axial strain becomes

$$\int_{-L}^{L}\frac{u_x^2}{2}\,dx = 2L\mathcal{E}. \tag{15}$$

The observed folding patterns are given by periodic stationary solutions u of the energy $\mathcal{W}$ and satisfying the end-shortening constraint (15). To the order of accuracy considered above the gradient flow equation (12) then becomes the nonlinear parabolic differential equation

$$-u_t = EI\left((2 - 5u_x^2)u_{xxxx} - 5u_{xx}^3 - 20u_xu_{xx}u_{xxx}\right) + Pu_{xx} - \frac{3}{2}(k_2h^2 + P)u_x^2u_{xx} + k_1u. \tag{16}$$

To give a stable solution we introduce the pinning condition

$$u(-L) = u'(-L) = u(L) = u'(L) = 0 \tag{17}$$

and then solve (16).

3.2. Amplitude equation derivation

We study this reduced system by using the multi-scale stability analysis used commonly to study the onset of periodic patterns [21], in which we set

$$u(x, t, X, T) = A(X, t, T)e^{i\omega x} + c.c \tag{18}$$

where X, T are assumed to be slow variables to be defined presently. If $|A|$ is *small* then to leading order A satisfies the linear fourth order differential equation

$$-A_t = (2EI\omega^4 - P\omega^2 + k_1)A \equiv \sigma A. \tag{19}$$

It is well known [21] that for P larger than a critical value the observed steady states solutions are also the most rapidly growing solutions of (19) over all possible values of the frequency ω. These satisfy the simultaneous equations

$$2EI\omega^4 - P\omega^2 + k_1 = 0, \quad \text{and} \quad 8EI\omega^3 - 2P\omega = 0 \tag{20}$$

Solving these gives the critical values

$$P = P_C = \sqrt{8EIk_1}, \quad \omega_C = \sqrt{\frac{P_C}{4EI}} = \left(\frac{k_1}{2EI}\right)^{1/4}. \tag{21}$$

with the critical period

$$\ell_C = 2\pi\left(\frac{2EI}{k_1}\right)^{1/4}. \tag{22}$$

The resulting small amplitude $|A|$ is then fixed by the linearised end-shortening condition (15) so that

$$2L|A|^2\omega_C^2 = 2L\mathcal{E} + O(1), \tag{23}$$

and therefore for large L we have the following measure of the solution amplitude in terms of the axial strain

$$|A| = \frac{\sqrt{\mathcal{E}}}{\omega_C}. \tag{24}$$

This calculation describes the onset of patterns at the critical axial load $P = P_C$, at infinitessimally small values of A. We now co nsider a more sophisticated multi-scale analysis to consider the more general case. For P close to P_C, $\sigma > 0$, we expect patterns of the form (18) for $|A|$ small and ω near ω_C to bifurcate from the basic state for $P - P_C \ll 1$. To capture amplitude and phase modulation of these patterns in this parameter range, we derive an envelope equation on slow time and space scales. The amplitude equation tells us not only what the patterns look like, but also gives us (in)stability information about the periodic patterns for certain parameter ranges. This is useful, since it helps us to locate the range of ω for which we expect to see stable patterns, without any implications from the boundary conditions.

To identify the appropriate temporal and spatial scales for the amplitude, and also the possible phase corrections, of the patterns close to the critical values of P_C and ω_C, we consider the dispersion relation (19) for $P - P_C = \epsilon^2 p$, $\omega = \omega_C + \epsilon^\gamma K$ where at this stage the small variable ϵ is simply a measure of the solution amplitude $|A|$ that we use to identify the correct scalings of P and ω. Then for $\epsilon \ll 1$ we have

$$-\sigma \sim 2EI(\omega_C^4 + 4\omega_C^3\epsilon^\gamma K + 6\omega_C^2\epsilon^{2\gamma}K^2) - (P_C + \epsilon^2 p)(\omega_C^2 + 2\omega_C\epsilon^\gamma K + \epsilon^{2\gamma}K^2) + k_1 \tag{25}$$

Using the definition of ω_c and P_c gives cancellation of the terms with coefficients that are $O(\epsilon^\gamma)$ or larger. Then balancing the remaining (leading order) contributions yields

$$\gamma = 1, \quad \sigma = O(\epsilon^2) \tag{26}$$

This result implies that it is appropriate to look for multiple scale behavior of the form, $u = u(x, t, X, T)$ for $X = \epsilon x$, $T = \epsilon^2 t$, and $P - P_C = \epsilon^2 p$, with ϵ^2 related to the end-shortening condition through the equation (24) so that

$$\epsilon^2 = \mathcal{E}/\omega_C^2. \tag{27}$$

With this ansatz, we have

$$\frac{\partial^n u}{\partial x^n} = \left(\frac{\partial}{\partial x} + \epsilon\frac{\partial}{\partial X}\right)^n u, \quad \frac{\partial u}{\partial t} = \left(\frac{\partial}{\partial t} + \epsilon^2\frac{\partial}{\partial T}\right)u, \tag{28}$$

so that equation (16) has the form

$$-u_t = L_0 u + \sum_{j=1}^{4} \epsilon^j N_j u \tag{29}$$

where $L_0 u = Lu$ with P replaced by P_c so that

$$L_0 u = 2EIu_{xxxx} + P_C u_{xx} + k_1 u \tag{30}$$

and the terms $N_j u$ may be nonlinear in u. Therefore we look for a perturbation expansion for u of the form

$$u \sim \epsilon u_1 + \epsilon^2 u_2 + \epsilon^2 u_3 + \ldots \tag{31}$$

The ϵ scaling of u_1 follows from the fact that we take $P = P_C + \epsilon^2 p$, and we expect patterns with small amplitude to bifurcate from the basic state with $p > 0$, see [21, pp. 285-305]. Furthermore, from the linear analysis above we see that σ is real, so that we expect stationary periodic patterns that bifurcate from the basic solution with evolution on the T time scale. Therefore we expect no fast time t dependence for this solution, that is, $u_j = u_j(x, X, T)$.

Substituting (31) in (29) and collecting like powers of ϵ yields

$$O(\epsilon): \qquad -L_0 u_1 = 0 \tag{32}$$

$$O(\epsilon^2): \qquad -L_0 u_2 = N_1 u_1 = 8EIu_{1xxxX} - 2P_C u_{1xX} \tag{33}$$

$$O(\epsilon^3): \qquad -L_0 u_3 = u_{1T} + N_2 u_1 + N_1 u_2 \tag{34}$$

As indicated from the dispersion relation (19) for $\sigma = \sigma(\omega, P)$ discussed above, we expect to find stationary patterns of the form $e^{i\omega_C x}$ with modulations on the long time scale T for P near to P_C. Therefore we conclude that

$$u_1 = A(X, T)e^{i\omega_C x} + \text{ c.c.} \tag{35}$$

Furthermore, given the relationship between ω_C and P_C above, $N_1 u_1 = 0$. Then we see that u_2 satisfies the same linear equation as u_1 and without loss of generality we can set $u_2 = 0$. Then,

$$\begin{aligned} -L_0 u_3 \quad = \quad & u_{1T} + 12EIu_{1xxXX} + P_C u_{1XX} + pu_{1xx} + EI[-5((u_{1x})^2 u_{1xxxx} \\ & -5(u_{1xx})^3 - 20u_{1x}u_{1xx}u_{1xxx}] - \frac{3}{2}(k_2 h^2 + P_C)(u_{1x})^2 u_{1xx} \end{aligned} \tag{36}$$

Using the expression for u_1 (35) yields terms of the form $C(X, T)e^{im\omega_C x}$ for $m = \pm 1, \pm 3$ on the right hand side of (36). Then we have a solvability condition for u_3 to eliminate the possibility of an unphysical solution that grows linearly with x,

$$\int_0^{2\pi/\omega_C} (u_{1T} + N_2 u_1)e^{\pm i\omega_C x} dx = 0 \tag{37}$$

Thus we find the coefficient of $e^{i\omega_C x}$ on the right hand side of (36) gives us the solvability condition which is the well-known Ginzburg Landau equation for $A(X, T)$ given by

$$A_T = \omega_C^2 pA + 2P_C A_{XX} + \omega_C^4 [10EI\omega_C^2 - \frac{3}{2}(k_2 h^2 + P_C)]|A|^2 A \tag{38}$$

Once again, note that at this stage we have not used the boundary condition $u = 0$, so (38) is capturing the general slow time and space modulation of a periodic pattern with wave number ω_C.

One simple non-trivial solution of (38) is given by taking $A = r_0$, where r_0 satisfies the equation

$$\omega_C^2 p + \omega_C^4[10EI\omega_C^2 - \frac{3}{2}(k_2h^2 + P_C)]r_0^2 = 0. \tag{39}$$

These solutions correspond to pure periodic solutions for $u(x)$. A further steady (in time) solution of (38) is given by a heteroclinic connection, which is in turn asymptotic to the periodic solutions of amplitude r_0. These both correspond to the desired folding patterns.

A standard linear stability analysis of simple solutions of this type with a possible shift in wave number $A = r_0 e^{i\omega_1 X}$ results in the well-known Eckhaus stability criterion for ω_1 [15], Then, the stability condition for solutions of (38) of the form $u \sim r_0 e^{i(\omega_C + \epsilon\omega_1)X}$ is

$$\omega_1^2 < \frac{\omega_C^2}{6P_C}\, p \tag{40}$$

Now, we consider how the boundary conditions contribute to the selection of certain periodic patterns within the possibilities indicated by (38) and (40). With the boundary conditions $u(\pm L) = u'(\pm L) = 0$ for $L \gg 2\pi/\omega_C$, we expect that the system selects periodic patterns $u \sim e^{i\omega x}$ on $-L < x < L$ with quantized wave number n satisfying $L\omega_L = n\pi$ for n an integer. Together with the condition (40), this observation indicates that for a stable pattern to exist, the selected wave number ω_L must be close to ω_C as $\epsilon \ll 1$. This observation in turn selects the appropriate integer n given by

$$n = \text{integer part of}\left(\frac{L\omega_C}{\pi}\right) \quad \text{and hence} \quad \omega_L = \frac{n\pi}{L}. \tag{41}$$

Additional analysis of the amplitude equation indicates that this wave number remains fixed in the weakly nonlinear parameter range [8]. To see this, we consider the possibility of stable amplitudes that vary in space $A = R(X)e^{i\Theta(X)}$, which would give phase corrections to $\omega_L X$. Substituting in (38), separating real and imaginary parts, and integrating the equations once yields

$$R^2\Theta'(X) = Q_1, \tag{42}$$

$$2P_C(R')^2 + 4P_C\frac{Q_1^2}{R} + \omega_C^2 pR^2 + \frac{\omega_C^4[20EI\omega_C^2 - 3(k_2h^2 + P_C)]}{4}R^4 = Q_2 \tag{43}$$

for Q_j, $j = 1, 2$ constant. With the boundary condition $u = 0$ it follows that $R = 0$ at some value of X. Then, in order to have bounded solutions, we must have that $Q_1 = 0$. As a result Θ = constant, and in the weakly nonlinear regime, the wave number is pinned at the value $\omega_L = L/(n\pi)$ for the integer n such that ω_L is as close as possible to ω_c.

We deduce that close to the critical point, the resulting solution takes the leading order form

$$u(x, X) = \epsilon R(X)e^{i\Theta}e^{i\omega_L x} + c.c.$$

In particular for small values of $\mathcal{E}$, apart from exponentially small corrections, we have the symmetric periodic solution

$$u(x) = 2\epsilon r_0 \cos(\omega_L x). \tag{44}$$

It follows from the end-shortening condition that

$$\epsilon r_0 = \frac{\sqrt{\mathcal{E}}}{\omega_L}. \tag{45}$$

From (39) and the condition that $P = P_C + \epsilon^2 p$ we then have that the axial load is given locally by

$$P = P_C + \omega_C^2 \left[-10EI\omega_C^2 + \frac{3}{2}(k_2 h^2 + P_C) \right] \epsilon^2 r_0^2 = P_C + \frac{\mathcal{E}\omega_C^2}{\omega_L^2} \left[-10EI\omega_C^2 + \frac{3}{2}(k_2 h^2 + P_C) \right] \quad (46)$$

We note that there is a critical value of $k_2 h^2 = k^*$ satisfying the identity

$$\frac{3}{2}(k^* + P_C) - 10EI\omega_C^2 = 0, \quad (47)$$

so that solutions exist in the super-critical range $P > P_C$ if $k_2 > k^*$ and the sub-critical range $P < P_C$ if $k_2 h^2 < k^*$. As $k_2 \gg 1$ for our system, it is only the super-critical case (for which the Eckhaus stability condition applies) which is of interest to us in this paper. We note further that for small values of $\mathcal{E}$ we have that P varies linearly with $\mathcal{E}$ but that ω is locally constant at ω_L. This situation changes for larger values of $\mathcal{E}$ and we study these in the next section.

4. Analysis of the fully nonlinear equation

4.1. Global bifurcations and large deviations

The analysis in the previous section establishes, for sufficiently large k_2, the existence of solution branches (u, P) parametrized by $\mathcal{E}$ with (locally) u and P increasing from the bifurcation point $(0, P_C)$ with increasing $\mathcal{E}$. In this section we now consider the fully nonlinear equation, without assuming $|u_x(x)|$ is small, and study the evolution of these branches away from the bifurcation points. Our starting point is therefore the fully nonlinear Lagrangian

$$W = \frac{EIu_{xx}^2}{(1+u_x^2)^{5/2}} + \frac{1}{2}k_1 u^2 + \frac{1}{2}k_2 h^2 \left(1 - \frac{1}{\sqrt{1+u_x^2}} \right)^2 - P\left(\sqrt{1+u_x^2(x)} - 1 \right). \quad (48)$$

We seek periodic energy minimising solutions of this Lagrangian (48), which we presume have a wavelength ℓ. This wavelength will be determined later as part of the solution, by using the end-shortening condition and stability arguments. To do this analysis, it is convenient to initially fix ℓ and to consider symmetric periodic solutions of period ℓ as functions of P, and to then find the end shortening $\mathcal{E}$.We will then return to determining P in terms of $\mathcal{E}$.

It follows that total potential energy of the periodic solution over the interval $[0, \ell]$ is given by

$$V(u,\ell) = \int_0^\ell W\, dx = \int_0^\ell EI\frac{u_{xx}^2}{(1+u_x^2)^{5/2}} + \frac{1}{2}\ell k_1 u^2 + \frac{1}{2}k_2 h^2 \left(1 - \frac{1}{\sqrt{1+u_x^2}} \right)^2 \quad (49)$$

$$-P\left(\sqrt{1+u_x^2(x)} - 1 \right) dx, \quad (50)$$

with the associated Euler-Lagrange equation

$$2EI\left[\frac{u_{xxxx}}{(1+u_x^2)^{5/2}} - 10\frac{u_x u_{xx} u_{xxx}}{(1+u_x^2)^{7/2}} - \frac{5}{2}\frac{u_{xx}^3}{(1+u_x^2)^{7/2}} + \frac{35}{2}\frac{u_{xx}^3 u_x^2}{(1+u_x^2)^{9/2}} \right]$$
$$+k_1 u + P\left[\frac{u_{xx}}{(1+u_x^2)^{1/2}} - \frac{u_x^2 u_{xx}}{(1+u_x^2)^{3/2}} \right] - k_2 h^2 u_{xx}\left[\frac{1}{(1+u_x^2)^{3/2}} - \frac{1}{(1+u_x^2)^{5/2}} \right]$$
$$-k_2 h^2 u_x^2 u_{xx}\left[\frac{3}{(1+u_x^2)^{5/2}} - \frac{5}{(1+u_x^2)^{7/2}} \right] = 0. \quad (51)$$

Periodic solutions of fourth order equations of the general form given by (51) have been studied in depth by many authors, and we refer to the monograph of [24] for a review of the genral theory for the existence, and certain aspects of the behaviour of, the periodic solutions of fourth order problems. Consequently we will only give a short description of the existence of the solutions for the equation in our case, as the main interest in this paper is the evolution of the (symmetric) periodic solutions towards the Chevron type folding patterns.

In particular, we see immediately that the Euler-Lagrange equations given by (51) are invariant under each of the reflectional symmetries $u \to -u$ and $x \to -x$ as well as translational symmetries in x. Our interest in this paper will be on solutions which inherit these symmetries both because this is the form of the solutions on the primary solution branch, and also because his study also significantly simplifies the subsequent analysis. Accordingly we fix the period ℓ of the periodic solution and consider solutions with all such reflectional symmetries. The function $u(x)$ will then be composed of two symmetrical half waves, identical up to a change in sign. We fix the phase of the first half wave by setting

$$u(0) = u''(0) = u(\ell/2) = u''(\ell/2) = 0, \tag{52}$$

We also consider those solutions with the symmetry

$$u(x) = u(\ell/4 - x). \tag{53}$$

On the half wavelength $[0, \ell/2]$ such solutions will then take the form

$$u(x) = \sum_{n\ odd} a_n \sin(2n\pi x/\ell) \tag{54}$$

We note that solutions of (51) which satisfy (52) and have the symmetry (53), can be extended to periodic solutions of the form (54) by odd periodic continuation. It is thus sufficient to study these for the case of ℓ fixed. We now establish the following

Lemma 1
Consider the solutions of the Euler-Lagrange equation (51) satisfying the boundary conditions given by (52)

(i) There exists a global solution branches bifurcating from the trivial solution at the bifurcation point $(u, P) = (0, P_C)$.,
(ii) The primary branch is symmetric about the centre-line of the domain, so that $u(x) = u(\ell/4-x)$ and thus the solutions on $[0, \ell/2]$ can be odd-periodically extended to periodic solutions on the whole real line.

Proof. (i) We set $v = u_{xx}$, then (51) may be cast into the form

$$\begin{aligned} & u_{xx} = v, \\ & 2EI\left[v_{xx} - 10\frac{u_x v v_x}{(1+u_x^2)} - \frac{5}{2}\frac{v^3}{(1+u_x^2)} + \frac{35}{2}\frac{v^3 u_x^2}{(1+u_x^2)^2}\right] \\ & +k_1 u(1+u_x^2)^{5/2} + P\left[v(1+u_x^2)^2 - u_x^2 v(1+u_x^2)\right] - k_2 h^2 v\left[(1+u_x^2) - 1\right] \\ & -k_2 h^2 u_x^2 v\left[3 - \frac{5}{(1+u_x^2)}\right] = 0, \end{aligned} \tag{55}$$

with boundary conditions

$$u(0) = u(\ell/2) = v(0) = v(\ell/2) = 0. \tag{56}$$

If L is then the compact integral operator given by the Greens function of the second derivative, we then have from (55,56) that

$$u = Lv \quad \text{and} \quad 2EIv = Lf(u, v, u_x, v_x; k_1, k_2, P) \tag{57}$$

where f is the nonlinear function given above. It is immediate from the previous analysis that if $P = P_C$ then this system has a simple eigenfunction given by

$$(u_{PC}(x), v_{PC}(x)) = (\sin(\omega_C x), -\omega_C^2 \sin(\omega_C x)). \tag{58}$$

The existence of a global solution branch bifurcating from the trivial solution then follows from the application of the methods of bifurcation theory for a nonlinear problem of the form (57) with a simple eigenfunction, as described in [7] Theorem 8.2. The required transversality condition for this theorem is satisfied if

$$\langle N_{P_c}\phi, \phi\rangle \neq 0$$

where N is the ordinary differential equation given in (51). For this particular case this amounts to the condition that

$$\int_0^{\ell/2} \sin^2(\omega_C x)\, dx \neq 0$$

which is naturally satisfied.

(ii) As observed earlier, the differential equation with boundary conditions given by (55,56) is invariant under the action of the reflectional symmetry $u(x) \to u(\ell/4 - x)$. This symmetry also leaves the simple eigenfunction given by (58) invariant The result follows from the Equivariant Branching Lemma [17], so that the bifurcating branch inherits the symmetry of the simple eigenfunction (56). □

4.2. Global analysis of the nonlinear equation in the limit of large k_2 and P

We now study the behaviour of periodic solution branches, obtained by the periodic extension of the solutions of (55,56), in the limit of large k_2 and $P = O(k_2 h^2)$. To do this we note that the Euler-Lagrange equation takes the form

$$\frac{d}{dx}\left[\frac{d}{dx}\left(\frac{\partial W}{\partial u_{xx}}\right) - \frac{\partial W}{\partial u_x}\right] + k_1 u = 0,$$

where the expression $\frac{\partial W}{\partial u_x}$ is linearly dependent upon P and k_2 and is hence large. Furthermore the higher order derivatives of u which will be expected to be large in boundary layers close to points of high curvature, only arise in the expression $\frac{d^2}{dx^2}\left(\frac{\partial W}{\partial u_{xx}}\right)$. Hence, in the limit of large P and k_2, the term $k_1 u^2$ in the expression for W arises at a lower order. We also note that the terms involving u_{xx} and higher order derivatives will only be important at isolated points of high curvature over small length scales. In particular we establish the existence of chevron type solutions using a phase plane analysis. In this calculation we will assume that ℓ is constant and consider the question of relating $\mathcal{E}$ to P.

Consequently, if in the limit of large P and k_2 we ignore the terms of the form $k_1 u^2$ then to leading order the Euler-Lagrange equation is given by

$$\frac{d}{dx}\left[\frac{d}{dx}\left(\frac{\partial W}{\partial u_{xx}}\right) - \frac{\partial W}{\partial u_x}\right] = 0.$$

This expression has an immediate first integral given by

$$\frac{d}{dx}\left(\frac{\partial W}{\partial u_{xx}}\right) - \frac{\partial W}{\partial u_x} = C,$$

for a suitable constant C. It follows, after some manipulation, that we then have

$$\frac{2EIu_{xxx}}{(1+u_x^2)^{5/2}} - \frac{5EIu_{xx}^2 u_x}{(1+u_x^2)^{7/2}} + \frac{Pu_x}{(1+u_x^2)^{1/2}} - k_2 h^2 u_x\left[\frac{1}{(1+u_x^2)^{3/2}} - \frac{1}{(1+u_x^2)^2}\right] = C. \tag{59}$$

Now, substituting $v = u_x$ into (59) and rearranging, gives the second order ODE

$$2EIv_{xx} - \frac{5EIv_x^2 v}{(1+v^2)} + Pv(1+v^2)^2 - k_2 h^2 v\left[(1+v^2) - (1+v^2)^{1/2}\right] = C(1+v^2)^{5/2}. \tag{60}$$

We can further simplify this equation using the following.

Lemma 2
On the primary symmetric periodic solution branch $C = 0$ and v thus satisfies the ordinary differential equation

$$2EIv_{xx} - \frac{5EIv_x^2 v}{(1+v^2)} + Pv(1+v^2)^2 - k_2 h^2 v\left[(1+v^2) - (1+v^2)^{1/2}\right] = 0. \tag{61}$$

Proof. On the primary solution branch we have the symmetry that $u(x) = u(\ell/2 - x)$. Thus, if $x = \ell/4$ we must have $u_x = u_{xxx} = 0$, and thus $v = v_{xx} = 0$. It follows immediately from (60) that $C = 0$. □

We now establish the possible existence of the fold bifurcation on this branch.

Lemma 3
For each fixed ℓ, the Equation (61) has no non-zero periodic solutions of period $\ell = 2\pi/\omega$, for sufficiently large P.

Proof. If P is very large, so that $P \gg k_2 h^2$, then by rewriting equation (61) as

$$2EIv_{xx} - \frac{5EIv_x^2 v}{(1+v^2)} + v(1+v^2)^2\left(P - k_2 h^2\left[\frac{1}{1+v^2} - \frac{1}{(1+v^2)^{3/2}}\right]\right) = 0. \tag{62}$$

and noting that $0 \le (1+v^2)^{-1} + (1+v^2)^{-3/2} \le 1$, then (61) can be closely approximated by the equation

$$2EIv_{xx} - \frac{5EIv_x^2 v}{(1+v^2)} + Pv(1+v^2)^2 = 0. \tag{63}$$

If we set $s = \sqrt{P}x$ then this becomes

$$2EIv_{ss} - \frac{5EIv_s^2 v}{(1+v^2)} + v(1+v^2)^2 = 0, \tag{64}$$

which we can write as the two-dimensional system in the phase-plane given by

$$\frac{dv}{ds} = w, \quad 2EI\,\frac{dw}{ds} = \frac{5EIw^2 v}{(1+v^2)} - v(1+v^2)^2.$$

This system has a number of symmetries, in particular $t \to -t, v \to -v$ and $t \to -t, w \to -w$, and the only singular point is at the origin.These symmetries imply that all solutions in the phase-plane are closed periodic orbits centred on the origin. If (v, w) are small then these orbits have period $2\pi/\sqrt{2EI}$. In contrast, if v and w are large then we can approximate it by

$$2EIv_{ss} - \frac{5EIv_s^2 v}{(1+v^2)} + v(1+v^2)^2 \approx 2EIv_{ss} + v(1+v^2)^2 = 0,$$

which has periodic solutions with a period which decreases (in proportion to $1/(1+v^2)$) as the amplitude of v increases. It follows from the continuity of the period of the periodic orbits that there is a *maximum* period T of *all* of the periodic orbits in the phase-plane. In Figure 3 we show the calculation of the half-period of the periodic solutions of (64) when $2EI = 1$ as a function of $v'(0) = \gamma$, taking $v(0) = 0$. In this figure we can clearly see this behaviour. It follows that as $s = \sqrt{P}x$ then the period of the solution in the x-variable is $T/\sqrt{P}$. For large P this must be less than ℓ and hence cannot be an ℓ-periodic solution of the original equation.

□

This result is fully consistent with the analysis of the next section which shows the existence of a fold bifurcation in the solution.

4.3. Phase-plane calculations of the chevron-type solutions

Now, we consider the case when P and k_2h^2 are both large and of comparable size, with $P < 4k_2h^2/27$, and will give a phase-plane base construction of the periodic solution of (61). We will show that in the phase-plane it is close to a heteroclinic orbit, corresponding to a chevron folding pattern, in which $v = du/dx$ is close to the constant values of $\pm v^*$, over most of the interval, with small regions of high curvature at $x = 0, \ell/2, \ell$ where $v = u_x = 0$. Initially we make the rescaling of $s = \sqrt{P}x$ to the differential equation (61) giving the system

$$\frac{dv}{ds} = w, \quad 2EI\,\frac{dw}{ds} = \frac{5EIw^2 v}{(1+v^2)} - v(1+v^2)^2 + \mu v\left[(1+v^2) - (1+v^2)^{1/2}\right], \tag{65}$$

where

$$\mu = \frac{k_2h^2}{P}. \tag{66}$$

We now show that for large P and appropriate values of μ, that the system (65) has *near heteroclinic* solutions corresponding to the chevron-type solutions described above.

We firstly study the singular points of (65). As well as the point $(v, w) = (0, 0)$ there are possible further singular points with $(v, w) \equiv (\pm v^*, 0)$ at the roots of the algebraic equation $F(\mu, v^*) = 0$ where

$$-v(1+v^2)^2 + \mu v\left[(1+v^2) - (1+v^2)^{1/2}\right] \equiv vF(\mu, v). \tag{67}$$

Close to these singular points, the behaviour of the solutions of (65) is given by the eigenvalues $\lambda_\pm$ of its linearisation. A simple calculation shows that these are given by

$$\lambda_\pm(\mu, v^*) = \pm\sqrt{v^* F_v(\mu, v^*)}. \tag{68}$$

Thus, the eigenvalues are imaginary and the singular point is a center, if $v^* F_v(\mu, v^*) < 0$, and the eigenvalues are real and take opposite signs, so that the singular point is a saddle, if $v^* F_v(\mu, v^*) > 0$. A simple calculation shows that

$$vF_v = v^2\gamma \equiv v^2(-4(1+v^2) + \mu(2 - 1/\sqrt{1+v^2}). \tag{69}$$

Setting $z^2 = 1 + (v^*)^2$ it follows immediately that $F(\mu, v^*) = 0$ if z satisfies the simple identity

$$z^3 = \mu(z-1). \tag{70}$$

A plot of z as a function of $1/\mu = P/k_2h^2$ is given in Figure 4 (a)
A simple analysis shows that this equation has no positive roots if $\mu < 27/4$ (so that $P > 4k_2h^2/27$) , a fold bifurcation if $\mu = \mu_F = 27/4$ at which point the single root is given by $z = 3/2$, and two real positive roots z_1, z_2 if $\mu > 27/4$ when $P < 4k_2h^2/27$. For large μ (or smaller P), these two roots are given to leading order by

$$z_1 = 1 + 1/\mu \ll z_2 = \sqrt{\mu}.$$

It follows from (69) that at these two roots we have

$$\gamma(z) = -4z^2 + \mu(2 - 1/z)$$

so that to leading order

$$\gamma(z_1) = 2\mu, \quad \gamma(z_2) = -2\mu.$$

Hence the smaller root at z_1 corresponds to a saddle-point and the larger root at z_2 to a centre. Exactly the same picture is given from symmetry when these roots are reflected. Hence, if $\mu > 27/4$ the phase plane takes the form illustrated in Figure 4 (b)
Note that $z_1 \approx 1 + 1/\mu$ implies that $v_1 \approx \sqrt{2/\mu}$. The implications of this analysis is that if $\mu > \mu_F$ so that

$$P < \frac{4}{27}k_2h^2$$

then there are two saddle points symmetric about the w-axis and, by symmetry, there exists a heteroclinic connection between the two roots at $v_- \approx -\sqrt{2/\mu}$ and $v_+ \approx \sqrt{2/\mu}$. Consider now the phase plane illustrated in Figure 4 (b). The periodic orbits close to the centre at the origin have

small amplitude and a half-period (in s) of approximately $\pi/\sqrt{2EI}$. These solutions correspond to the small amplitude sinusoidal periodic orbits close to the primary bifurcation points P_1. As P increases it follows from the identity $s = \sqrt{P}x$ that the periodic orbits increase in period, and as P gets very large they increase in amplitude and converge towards the heteroclinic connection. On rescaling this corresponds to a chevron folding pattern in which the gradient of the solution $v(x) = u'(x)$ changes from v^* to $-v^*$ over a region of width $O(1/\sqrt{P})$. We also note that the predicted value of the fold P_F is given when

$$P_F/k_2h^2 = 4/27.$$

4.4. Kink band solutions

We can repeat this leading order calculation for the case of $C > 0$ in (60). The phase plane for (73) then has fixed points at $(v^+, 0)$ and $(-v^-, 0)$ In this case we have near *homoclinic* solutions which spend most of the period close to the fixed point at $(v^+, 0)$ with shorter periods close to the point at $(v^-, 0)$. When integrated the function $u(x)$ then has a *kink-band form* in which it increases overall with periods of positive slope with gradient close to v^+ and shorter periods of negative slope with gradient close to $-v^-$. It is intriguing to note that as well as chevron type solutions, these kink-band like geometries are (at least locally) energy minimising arrangements of vertical stacking identical layers, and at least geometrically are typical of kink bands observed in exposed escarpments of folds as well as in experiments on layers of paper [25, 32, 20]. However, the physical significance of these solutions in the context of this model is unclear; since contributions of inter-layer shear are neglected, which is known to play a fundamental role in the initiation and growth of kink bands [20]. We will study such kink bands, which also involve shear, in a future paper.

4.5. The validity of the leading order solution

We briefly consider now the effects of omitting the term k_1u in these calculations. It is easiest to consider this with respect to the reduced model which has all of the essential features of the original and has very similar solutions. With a simplified scaling this gives

$$u'''' + Pu'' - \frac{3}{2}(P + k_2h^2)u''(u')^2 + k_1u = 0. \tag{71}$$

This can be expressed as:

$$(v'' + Pv - \frac{1}{2}(P + k_2h^2)v^3)' + k_1u = 0, \quad u' = v. \tag{72}$$

We follow the previous reasoning and assume that P is large and that v'' may also be large. Thus to leading order, envoking symmetry and periodicity, we have:

$$v'' + Pv - \frac{1}{2}(P + k_2h^2)v^3 = 0. \tag{73}$$

The equation (73) admits small amplitude periodic solutions of period $O(1/\sqrt{P})$. It also admits larger amplitude near *heteroclinic* solutions of period tending to infinity when the largest value of v^2 is

$$v^2_{max} = \frac{2P}{P + k_2h^2}.$$

The heteroclinic solution $v_H(x)$ and its integral $u_H(x)$ (of chevron form), are then (up to translation) given by

$$v_H(x) = \frac{\sqrt{2}}{\sqrt{1 + k_2 h^2/P}} \tanh(\sqrt{P}x/2), \quad u_H(x) = \frac{8}{\sqrt{P + k_2 h^2}} \log(\cosh(\sqrt{P}x/2)). \tag{74}$$

Consider now the problem (72). If the leading order solution for v is as above, then we will have chevron type solutions for u of maximum amplitude $v_{max}\ell/4$ where ℓ is the period. Furthermore, over one half-period we have that

$$\int_0^{\ell/2} u \, dx = \int_{\ell/2}^{\ell} u \, dx = 0.$$

Hence the cumulative perturbative effect of u on the solution for v is both small (of order $1/P$) and averages to zero over any half-period.

5. End-shortening and wavelength selection for the chevron folds

The analysis of the previous section in identifying the relation between chevron folds and near heteroclinic orbits gives a link through (70) between the axial load P and the slope $u' = v^*$ of the fold. We now make clear the links in this case between P and the axial strain $\mathcal{E}$, the solution wavelength ℓ and the solution amplitude a.

5.1. Relations between wavelength, slope and amplitude

In the primary bifurcation at $P = P_C$ and $\mathcal{E} = 0$ we observe a periodic solution $u(x)$ of period close to ℓ_C proportional to $1/\sqrt{P_C}$ so that $u'(0) = u'(\ell_C/2) = u'(\ell_C)$ and $u(x) \approx a\cos(2\pi x/\ell)$ with $\sqrt{a}$ proportional to $\mathcal{E}$ or $P - P_C$. As P and $\mathcal{E}$ increase, so the solution evolves to the chevron fold in which $u'(0) = u'(\ell/2) = u'(\ell)$ and we have

$$u'(x) \approx -v^* \quad \text{if} \quad 1/\sqrt{P} \ll x \ll \ell/2 - 1/\sqrt{P} \quad \text{and} \quad u'(x) \approx v^* \quad \text{if} \quad \ell/2 + 1/\sqrt{P} \ll x \ll \ell - 1/\sqrt{P}.$$

To make this calculation slightly more precise we note that in the rescaled coordinates the rescaled horizontal variable is $s = \sqrt{P}x$. The horizontal distance $x \in [0, H]$ occupied by half of the chevron fold is given by $H = \ell/2$ and in rescaled coordinates it takes a 'time' of

$$S = \sqrt{P}\ell/2 \tag{75}$$

to traverse the orbit. As the orbit is close to a heteroclinic connection joining $(-v^*, 0)$ to $(v^*, 0)$ it follows that if it approaches to within a distance ϵ of the fixed saddle-point, so that $-v^* + \epsilon < v < v^* - \epsilon$ then it takes $O(1)$ time to move in the phase-plane between the saddle-points, corresponding to $O(1/\sqrt{P})$ in unscaled coordinates, and a time of $O(\log(1/\epsilon))$ to move in the part of the phase-plane close to the saddle-points. It then follows from (75) that

$$\log(1/\epsilon) \sim \sqrt{P}\ell/2, \quad \ell \sim \log(1/\epsilon)/\sqrt{P}$$

so that

$$\epsilon \sim e^{-\sqrt{P}\ell/2}. \tag{76}$$

Thus we have that ϵ is very small for large P and that consequently the solution is very close to the chevron form, of slope $v = \pm v^*$. This to a certain extent justifies the previous analysis.

It is immediate that the amplitude a of the chevron fold is given by

$$a = \frac{(\ell - O(1/\sqrt{P}))}{4}\,(v^* - O(\epsilon))\,. \tag{77}$$

An example of a typical chevron fold (taken over 3 full periods), showing the limbs and the region of high curvature is given in Figure 5

5.2. End-shortening

We will now assume that the long layer of length $2L$ under the effect of the increasing end-shortening (and hence increasing load) buckles into the concertina shape illustrated in Figure 5 with N chevron patterns, each comprising 2 straight limbs of constant gradient u'. Here N is initially unknown. The length of each such limb is then given by $2L/2N = L/N$ together with a correction of order $1/\sqrt{P}$ which we will ignore for this section. The following lemma then describes the geometry of the chevron fold.

Lemma 4

If we consider a pure chevron fold comprising N patterns, each with 2 *straight limbs of slope* $u' = \pm v^*$*, then*

(i) The horizontal length of each straight limb is given by

$$L/(N\sqrt{1+u'^2}) \quad \textit{so that the period of each chevron pattern is} \quad \ell = 2L/(N\sqrt{1+u'^2}). \tag{78}$$

(ii) The total end-shortening is independent of *N and is given by*

$$2L\mathcal{E} = 2L - 2L/\sqrt{1+(v^*)^2} = 2L(1-1/z) \quad \textit{so that} \quad \mathcal{E} = \frac{z-1}{z}, \tag{79}$$

where z is as given in the previous section and takes the value

$$z = \sqrt{1+(v^*)^2}. \tag{80}$$

The proof of this lemma is immediate from the geometry of the fold. The significance of this result is the fact that v^* and hence z is determined from the nature of the heteroclinic orbit studied in the previous section. It follows that (again ignoring terms of order $1/\sqrt{P}$) we have

$$z = \frac{1}{1-\mathcal{E}} \quad \text{so that} \quad |u'| = v^* = \sqrt{\frac{1}{(1-\mathcal{E})^2} - 1}. \tag{81}$$

Furthermore, from (70) we also have

$$z^3 = \mu(z-1), \quad \mu = \frac{k_2 h^2}{P}. \tag{82}$$

It then follows from (82) that

$$\frac{1}{(1-\mathcal{E})^3} = \mu\left[\frac{1}{(1-\mathcal{E})} - 1\right].$$

Rearranging this expression, it follows that on a chevron fold we have the following relation between P and $\mathcal{E}$ given by

$$P = k_2 h^2 \left[(1-\mathcal{E})^2 - (1-\mathcal{E})^3 \right]. \tag{83}$$

Note that under compression we expect to see $\mathcal{E}$ increase from zero to a maximum value of one. The maximum value of the right hand side of (83) is given when

$$2(1-\mathcal{E}) = 3(1-\mathcal{E})^2$$

so that

$$\mathcal{E} = 1/3 \quad \text{and} \quad P = 4k_2 h^2/27, \tag{84}$$

i.e. there is a maximum value of $P = P_F = 4k_2 h^2/27$ which will be observed as a fold bifurcation.

5.3. Wavelength selection

Although we can find P in terms of $\mathcal{E}$, the value of N and hence of ℓ is unknown. We conjecture that the total number of folds *remains constant* throughout the evolution of the chevron folds, and hence $N = n$ where n given by the expression (41) at the bifurcation point is given by the integer part of $L\omega_C/\pi$. In this case we conclude that

$$\ell = \frac{2L}{n\sqrt{1+(v^*)^2}} = \frac{2L}{n}(1-\mathcal{E}), \tag{85}$$

with v^* given by (80,82).

6. Numerical Results

6.1. Fold initiation

For the first calculation of the fold initiation we consider a solution $u(x,t)$ of the time-dependent Swift-Hohenberg equation

$$\frac{\partial u}{\partial t} = -\frac{\delta W}{\delta u} := -f(P,u) \quad \text{subject to the rigid loading constraint} \quad \frac{1}{2L}\int_{-L}^{L} u'^2 \, dx = \mathcal{E} \tag{86}$$

and let u and P evolve with time towards a steady solution for a fixed axial strain $\mathcal{E}$. We solve (86) using finite elements over a large-but-finite domain $X := [-L, L]$. In order to obtain a stable solution it is necessary to impose a weak pinning of the solution given by taking

$$u(-L,t) = u(L,t) = 0, \quad u'(-L,t) = u'(L,t) \quad \text{with} \quad L = 40,$$

The weak form is found by multiplying by a suitable test function v, integrating over the domain X and then by parts, giving

$$\int_X \dot{u}v \, \mathrm{d}x = -\int_X f(P,u)v \, \mathrm{d}x. \tag{87}$$

The domain X is discretized into N nodes $x_i = ih - L$ where $h = 2L/N$ and $i = 0, 1, \ldots, N$. Since the weak form contains second derivatives of u and v, the solution is interpolated with piecewise

cubic shape functions. Each node has two degrees of freedom (u_i and u_i') and the approximate finite solution over the i^{th} element $x \in [x_i, x_{i+1}]$ is given by

$$u_h(t) = u_i(t)\phi_i + u_{i+1}(t)\phi_{i+1} + u_i'(t)\phi_{N+i} + u_{i+1}'(t)\phi_{N+i+1} \tag{88}$$

where if $s = (x - x_i)/(x_{i+1} - x_i)$ then

$$\phi_i = 2s^3 - 3s^2 + 1 \quad \phi_{i+1} = s^3 - 2s^2 + s \quad \phi_{N+i} = -2s^3 + 3s^2 \quad \text{and} \quad \phi_{N+i+1} = s^3 - s^2 \tag{89}$$

and all other $\phi_j = 0$ for $x \in [x_i, x_{i+1}]$. The nodal degrees of freedom are collected in a single vector $\underline{U}(t) = (u_1(t), \ldots, u_{N-1}(t), u_0'(t), \ldots, u_N'(t))^T$, so that finite element solutions of (87) are solutions of the system of equations

$$\mathbf{A}\dot{\underline{U}} = -\underline{F}(P, \underline{U}) \quad \text{such that} \quad \frac{1}{2L}\underline{U}^T\mathbf{C}\underline{U} = \mathcal{E} \tag{90}$$

where the matrices and vectors are defined as follows:

$$\mathbf{A}_{ij} = \int_X \phi_i\phi_j \, dx, \quad \mathbf{C}_{ij} = \int_X \phi_i'\phi_j' \, dx, \quad F_i = \int_X f(P, \underline{U})\phi_i \, dx. \tag{91}$$

In order the generate a system of DAEs of order 1, we first by differentiate the constraint equation, $\frac{1}{2L}\underline{U}^T\mathbf{C}\underline{U} = \mathcal{E}$ with respect to time so

$$\underline{U}^T\mathbf{C}\dot{\underline{U}} = 0. \tag{92}$$

Thus the numerical reduction of the constrained Swift-Hohenberg equation (86) to a system of DAEs is

$$\begin{bmatrix} U^T\mathbf{C} & 0 \\ \mathbf{A} & 0 \end{bmatrix}\begin{bmatrix} \dot{U} \\ \dot{P} \end{bmatrix} = \begin{bmatrix} 0 \\ -\underline{F} \end{bmatrix}. \tag{93}$$

Such index-1 DAEs can be solved using MATLAB's function `ode23s`. In practise stationary solution are achieved by providing an initial guess of the solution with the correct axial strain $\mathcal{E}$. The equation (93) is then solved over a long time until equilibrium is achieved. Letting $EI = k_1 = 1$ and taking $k_2h^2 = 100$, the results of this calculation are presented in Figures 6 and 7,where we plot the solution amplitude a, the axial load P and the frequency ω as functions of $\mathcal{E} = \Delta/L$.

The results in Figure 6 are exactly as predicted by the weakly nonlinear analysis with $P_C = \sqrt{8k_1EI} = \sqrt{8} \approx 2.828$ and the linear dependence of P on $\mathcal{E}$ predicted by (46). In Figure 7 we see the effects of the weak pinning. The value of $\omega_C = (k_1/2EI)^{1/4} = 0.8409$ given by the initial linear analysis is slightly less than the observed value at the bifurcation. However, noting that the pinning length is $L = 40$ we have that $L\omega_C/\pi = 10.7$. Hence from the expression (41) the nearest integer wave number is $n = 11$. Consequently from (41) we have

$$\omega_L = \frac{n\pi}{L} = \frac{11\pi}{40} = 0.8639$$

which is the observed value and is as predicted by the amplitude equation calculation in Section 3. As predicted, this value is *pinned* and stays very close to constant as $\mathcal{E}$ varies. This pinning continues until $\mathcal{E} \approx 0.07$ For larger values of $\mathcal{E}$ we see a nonlinear change as predicted by the fully nonlinear analysis

6.2. Development of the chevron folds

We now make some computations of a half-period of the first solution branch (on which the solution is positive) and consider the effects of taking both P and k_2 large. It is difficult numerically to use the finite element method for the fully nonlinear time dependent calculation. Accordingly we will simplify our calculations by taking the half-period of the solution to be fixed at $\ell/2 = 1$ and consider the dead loading case in which P increases. This calculation is reasonable as our primary objective is to show the development of the chevron folds in this case

The solution branches to (51) for a fixed half wavelength $\ell/2 = 1$ are readily computed from the trivial state as P increases by using the collocation based continuation package for systems of ODEs `auto` ([9]). In this calculation P is increased from zero until the bifurcation point at P_C is encountered. The solution branch is then switched and the solution continued into and through the observed fold bifurcation. Alternatively the solution can be determined using the collocation based Matlab routine `bvp4c`. In this case an initial guess is needed for the solution. We find that the initial guess $u(x) = a\sin(\pi x)$ works well provided that a is taken to be the value given by the Lyapunov-Schmidt solution approximation described in Section 3. The analysis of Section 4 guides us in the manner of the simplest discretisation of this system. We note that that fourth order ODE problem has the form

$$\frac{d}{dx}\left(\frac{d}{dx}\left(\frac{\partial W}{\partial u_{xx}}\right) - \frac{\partial W}{\partial u_x}\right) + k_1 u = 0$$

with the first part of this expression being dominant. Accordingly we solve the system

$$\frac{d}{dx}\left(\frac{\partial W}{\partial u_{xx}}\right) - \frac{\partial W}{\partial u_x} = y, \quad \frac{dy}{dx} = -k_1 u,$$

with

$$u(0) = u(1) = u_{xx}(0) = u_{xx}(1) = 0.$$

In Figure 8 we show two solution branches of the periodic solutions of this full system in the two cases of (a) $k_2h^2 < k^*$ where locally $P < P_C$ and (b) $k_2h^2 > k^*$ where locally $P > P_C$ (see equation (47)). Firstly we note that the local bifurcation analysis predicts that in this case $P_C = 2\pi^2 - 1/\pi^2 = 19.8$. Prominent in Figure 8 (b) is the predicted fold bifurcation at $P = P_F$, indicating the non-existence of a periodic solution for sufficiently large P. We can compare this figure with the theoretical Figure 4 (a) showing the location of the saddle-point in the phase plane as a function of $1/\mu = P/(k_2h^2)$ and we see close correspondence. By calculating P_F for increasing values of k_2, Fig. 8 (right), we observe that as $k_2 \to \infty$ the ratio of $1/\mu_F = P_F/k_2h^2 \to 1/\mu^*$ a constant close to the predicted value of $4/27$.

In Figure 9 we show the solution profiles for a half-wavelength (x, u) (top row) and in the (u_x, u_{xx}) phase-plane (bottom row) for increasing values of $P^C \le P \le P_F$ (with each plot) and of k_2h^2 (from left to right). Firstly, observe as predicted, that all of these positive solutions have a reflectional symmetry. Secondly, we see for moderate values of k_2 the solution profile is approximately sinusoidal for both small and moderate values of P. However, this situation changes significantly when both k_2h^2 and P are *both* large. In particular we note that in the case of large k_2 and large $P \simeq P_F$, Fig. 9 (right), solutions form a heteroclinic connection in u_x leading to a chevron type solution in (x, u), characterised by the expected straight limbs of slope $\pm v^*$ connected by a region of large curvature over a small length-scale $\epsilon \approx 1/\sqrt{P}$. The phase-plane clearly shows the evolution of the small amplitude periodic solution to the near heteroclinic orbit.

We also include a series of calculations made with the Matlab routine bvp4c for the particular case of $P = 600$ and $k_2h^2 = 10000$ for which $1/\mu = 0.06$ and it follows from the earlier analysis and formulas (80) and (82) that the saddle point occurs when $z = \sqrt{1+u'^2} = 1.0744$, so that the predicted maximum value of $|u'| = 0.3929$. In these calculations we find that the calculated maximum value of $|u'| = 0.3928$ very close to the predicted value. The resulting functions $u(x), u'(x)$ and $u''(x)$ taken over 3 full periods (so that $x \in [0, 6]$) and the resulting (u', u'') phase plane are given in Fig. 10.
We can compare these figures with the chevron folds at Millook Haven shown in Fig. 11.

7. Concluding remarks

In this paper we present a simplified energy-based model, to investigate the role geometry plays in fold pattern selection, when layers of rock are buckled from an initially flat state into chevron folds. The novel feature, which distinguishes this model from earlier analysis, is the inclusion of the elastic material of modulus $k_2 \gg 1$ between the two stiff layers. By doing this we are able to observe a smooth transition from sinusoidal to chevron type folding patterns as the axial strain and axial load are increased, and we can predict many of the features of the resulting chevron folds by using a phase-plane analysis. The overall argument leading to this solution links the existence of the chevron folding patterns of straight limbs separated by small regions of high curvature, to a near heteroclinic orbit in the (u', u'') phase plane in which $|u'|$ is constant over much of the range, apart from regions of with $O(1/\sqrt{P}) \ll 1$. This argument is reasonably robust to the fine details of the model used. Indeed the key feature is the existence of a constant (absolute) slope solution $|u'|$ to the equation $d/dx(\partial W/\partial u_x))$ in which we see a balance between the axial load P the slope u' and the elastic forces proportional to k_2. We will develop more sophisticated models including shear in a future paper, which will also look at the existence of kink bands. However, we expect to see a similar link in these cases between heteroclinic (or in the case of kink bands, homoclinic) orbits in the phase plane and many rock folding patterns involving regions of constant slope separated by regions of high curvature.

ACKNOWLEDGEMENTS We would like to acknowledge the support of the FP7 Marie-Curie ITN FIRST, the Pacific Institute for Mathematics Sciences (PIMS) and the NSERC Discovery Grant for the funding of the research described in this paper.

[1] Adhikary, D.P. & Dyskin, A. V. (1997) A Cosserat Continuum Model for Layered Materials, *Computers and Geotechnics,* **20**:15-45.
[2] Biot, M. A. (1961) Theory of folding of stratified viscoelastic media and its implications in tectonics and orogenesis, *Geol. Soc. America Bull.* **72**:1596-1620.
[3] Biot, M. A. (1963) Internal buckling under finite strain, *Proc. Roy. Soc. Lond. A* **273**:306-328.
[4] Biot, M. A. (1964) Theory of internal buckling of a confined multilayered structure, *Geological Society of America Bulletin,* **75**:563-568, doi:10.1130/0016-7606.
[5] Boon, J. A., Budd C. J. & Hunt, G. W. (2007) Level set methods for the displacement of layered materials, *Proc. R. Soc. Lond. A*, **462**:1447-1466, doi:10.1098/rspa.2007.1827.
[6] Budd, C. J., Edmunds, R. & Hunt, G. W. (2003), A nonlinear model for parallel folding with friction, *Proc. R. Soc. Lond. A* **459**:2097-2119, doi:10.1098/rspa.2003.1139.
[7] Chow, S-N, & Hale, J.K. (1982), Methods of Bifurcation Theory, Springer-Verlag.
[8] Cross, M.C., Daniels, P.G., Hohenberg,P.C., and Siggia, E.D. (1980), Effect of Distant Side Walls on Wave-Number Selection in Rayleigh-Benard Convection, *Phys. Rev. Let.*, **45**: 898-901
[9] Doedel, E. J., Paffenroth, R. C., Champneys, A.R., Fairgrieve, T. F., Kuzetsov, Y. A., Oldeman, B. E., Sandstede, B. & Wang, X. (2002) AUTO 2000: Continuation and bifurcation software for ordinary differential equations (with HomCont).*Technical Report, Concordia University, Montreal.*

[10] Dodwell, T. J., Peletier, M. A., Budd, C. J. & Hunt, G. W. (2012a), Self-Similar Voiding Solutions of a Single Layered Model of Folding Rocks, *SIAM J. Appl. Math.,* **72**:444-463, doi:10.1137/110822499
[11] Dodwell, T. J., Hunt, G. W., Peletier, M. A. & Budd, C. J. (2012b), Multi-layered folding with voids *Phil. Trans. Roy. Soc. A* **370**:1740-1758, doi:10.1098/rsta.2011.0340
[12] Dodwell, T. J. & Hunt, G. W. (2012c), Convoluted accommodation structures in folded rocks, *Phil. Mag.* **92**:3418-3438, doi:10.1080/14786435.2012.685771
[13] Dodwell, T. J., Butler, R. & Hunt, G. W. (2014), Out-of-plane ply wrinkling defects during consolidation over a an external radius, *Compos. Sci Technol.* **104**:151-159, doi:10.1016/j.compscitech.2014.10.007
[14] Dodwell, T. J. (2015), Internal wrinkling instabilities in layered media, Philosophical Magazine, 95:28-30, 3225-3243, DOI: 10.1080/14786435.2015.1034221
[15] Eckhaus, W.. (1965), Studies in Nonlinear Stability Theory, Springer-Verlag
[16] Frehner, M. & Schmalholz, S. M. (2006) Numerical simulations of parasitic folding in multilayers, *Journal of Structural Geology,* **28**:1647-1657, doi:10.1016/j.jsg.2006.05.008
[17] Golubitsky, M., Steward, I. & Schaeffer, D. G. (1988), Singularities and Groups in Bifurcation Theory, *Volume II. Springer-Verlag, New York.*
[18] Hobbs, B. E., Means, W. D. & Williams, P. F. (1976), An outline of structural geology, *John Wiley and Sons.*
[19] Hunt, G.W., Peletier, M. A., Champneys, A. R., Woods, P. D., Wadee M., Budd, C. J. & Lord, G. (2000) Cellular Buckling in Long Structures, *Nonlinear Dynamics*, **21**:3-29.
[20] Hunt, G. W., Dodwell, T. J. & Hammond, J. (2013) On the nucleation and growth of kink and shear bands, *Phil. Trans. R. Soc. Lond. A,* **371**:20120431, doi:10.1098/rsta.2012.0431
[21] Manneville, P. (1990), Dissipative structures and weak turbulence, in *Perspectives in Physics*, Academic Press.
[22] Muhlhaus, H. B. (1991), Continuum models for layered and blocky rock, *in Comprehensive Rock Engineering, Vol 2: Analysis and Design Methods, Pergamon Press, Oxford.*
[23] Peletier, M. A. (2001) Sequential Buckling: A Variational Analysis, *SIAM Journal on Mathematical Analysis*, **32**:1142-1168.
[24] Peletier, L. A. & Troy,W.C (2001) Spatial Patterns, Higher Order Models in Physics and Mechanics, Birkhauser.
[25] Price, N. J. & Cosgrove, J. W. (1990), Analysis of Geological Structures, *Cambridge University Press*.
[26] Rabinowitz, P. (1978) Periodic solutions of Hamiltonian systems, *Comm. Pure Appl. Math.*, **31**:157184.
[27] Ramberg, H. (1964), Selective buckling of composite layers with constrasted rheological properties, a theory for simultaneous formation of several orders of folds, *Tectonophysics* **1**:207-341, doi:10.1016/0040-1951(64)90020-4
[28] Ramberg, H. (1970), Folding of laterally compressed multilayers in the field of gravity, *Physics of the Earth and Planetary Interiors* **2**:203-232, doi:10.1016/0031-9201(70)90010-5
[29] Ramsay, J (1974), Development of chevron folds, *Geological Society of America Bulletin*, **85**:1741-1754, doi:10.1130/0016-7606
[30] Schmalholz, S. M. & Schmid, D. W. (2012). Folding in power-law viscous multi-layers. *Phil. Trans. Roy. Soc. A*, **370**:1798- 1826, doi: 10.1098/rsta.2011.0421
[31] Thompson, J. M. T. & Hunt, G. W. (1973), A general theory of elastic stability, *Wiley, London.*
[32] Wadee, M. A., Hunt, G. W. & Peletier, M. A. (2004), Kink band instability in layered structures, *J. Mech. Phys. Solids* **52**:1071-1091, doi:10.1016/j.jmps.2003.09.026

Figure 1: Folded, layers of rocks (Left) Smooth folds at Adamello, Italy (Right) Chevron type folds observed folds at Kangaroo Island, Australia. Pictures courtesy of Bruce Hobbs.

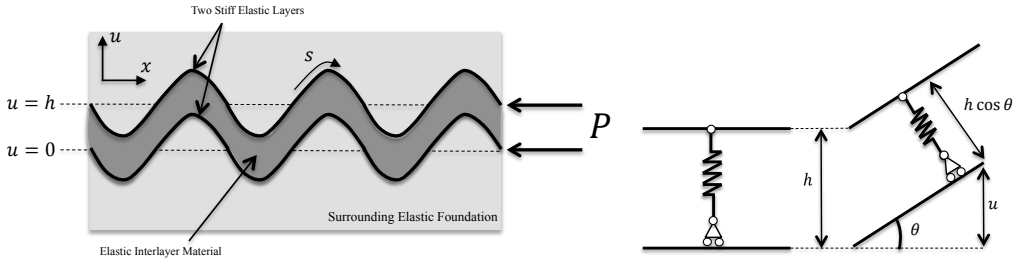

Figure 2: (Left) Two identical, stiff layers separated by an elastic medium, considered as part of a much larger vertically periodic multilayered system. It is assumed that the displacement of the two layers are related by the vector translation $(0, h)$. (Right) Elastic interlayer material is model by a series of linear elastic springs of stiffness $k_2 \gg 1$, which is constrained to remain perpendicular as the layers before.

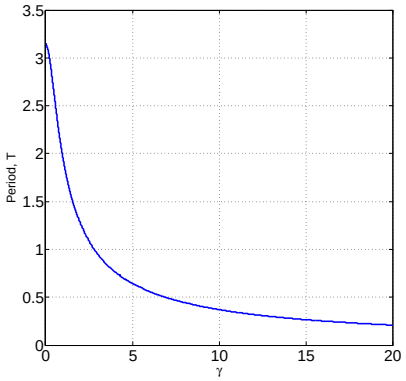

Figure 3: The half-period of the solutions of (64) when $2EI = 1$, $v(0) = 0$ as a function of $\gamma = v'(0)$.

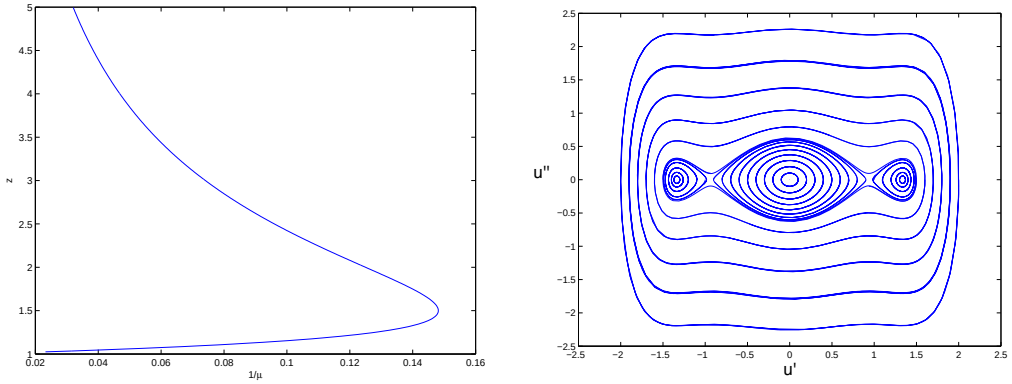

Figure 4: (a) The value of z plotted as a function of $1/\mu = P/k_2h^2$ showing a fold bifurcation when $1/\mu = 4/27$ and $z = 3/2$, (b) The (u', u'') phase plane if $\mu > 27/4$.

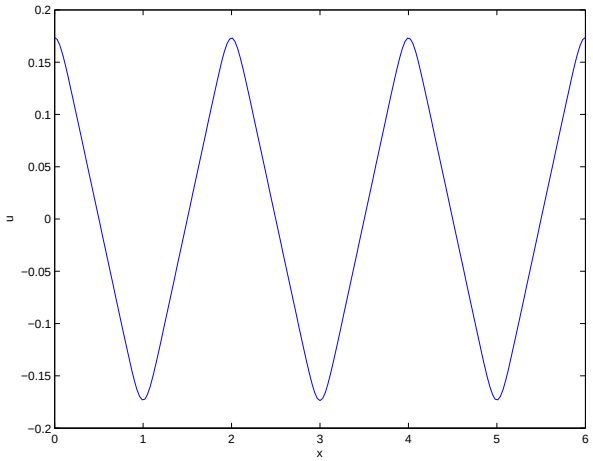

Figure 5: A typical profile of a chevron fold.

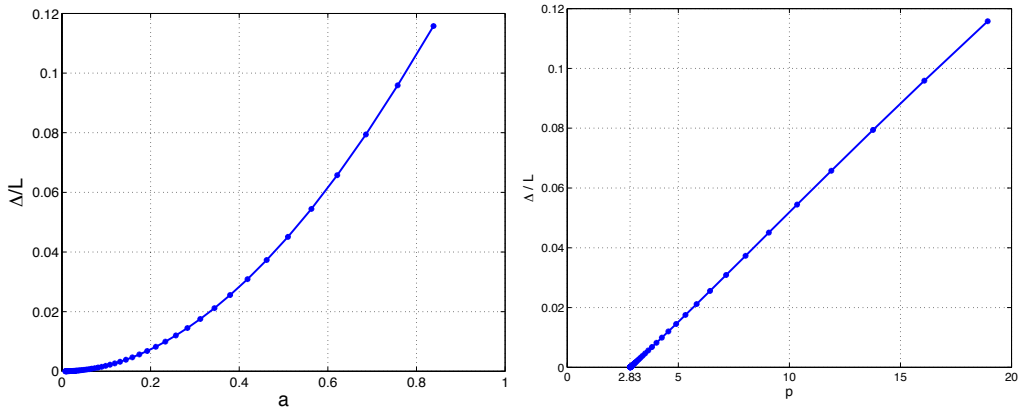

Figure 6: (left) The evolution of the solution amplitude with $\mathcal{E}$ showing the expected relation of a proportional to $\mathcal{E}^2$. (right) The evolution of the axial load P. Note the bifurcation from $P_C = \sqrt{8k_1 EI}$ with the predicted linear dependence on $\mathcal{E}$ given by (46).

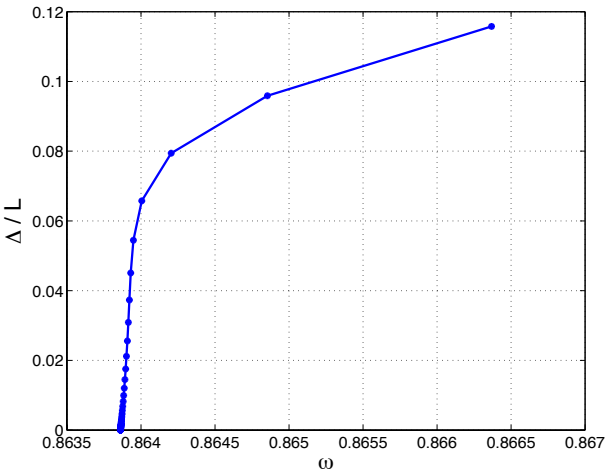

Figure 7: The evolution of the solution frequency ω with $\mathcal{E}$. Note the pinning of this value at ω_L close to the value of $\omega_C = \frac{11\pi}{40} = 0.8639$ over a range of values of $\mathcal{E}$.

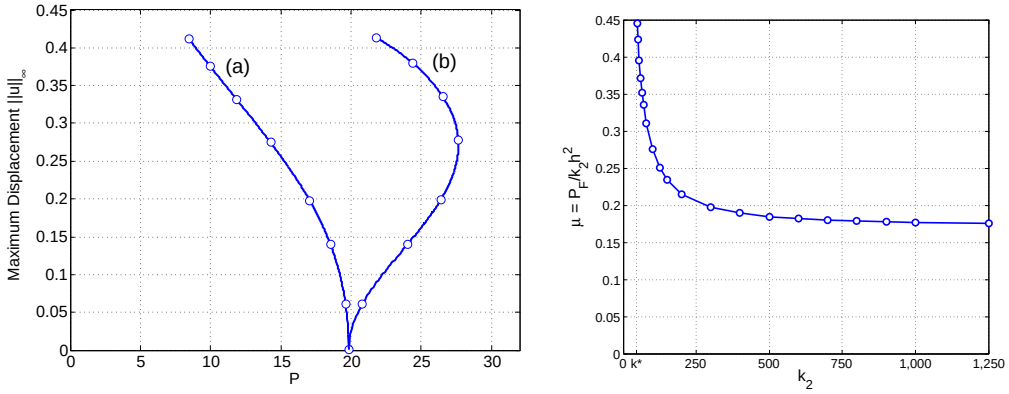

Figure 8: (Left) Solutions branches in $(P, \|u\|_\infty)$ space: (a) $k_2h^2 = 10 < k^*$, (b) $k_2h^2 = 100 > k^*$. Solution branch (b) shows a fold bifurcation at $P = P_F \approx 27.5$. (Right) A plot of k_2 against $1/\mu = P_F/k_2h^2$. In particular we note that as $k_2 \to \infty$, then $1/\mu \to 0.17$. In both plots we set $EI = k_1 = \ell/2 = 1$, and these values remain constant.

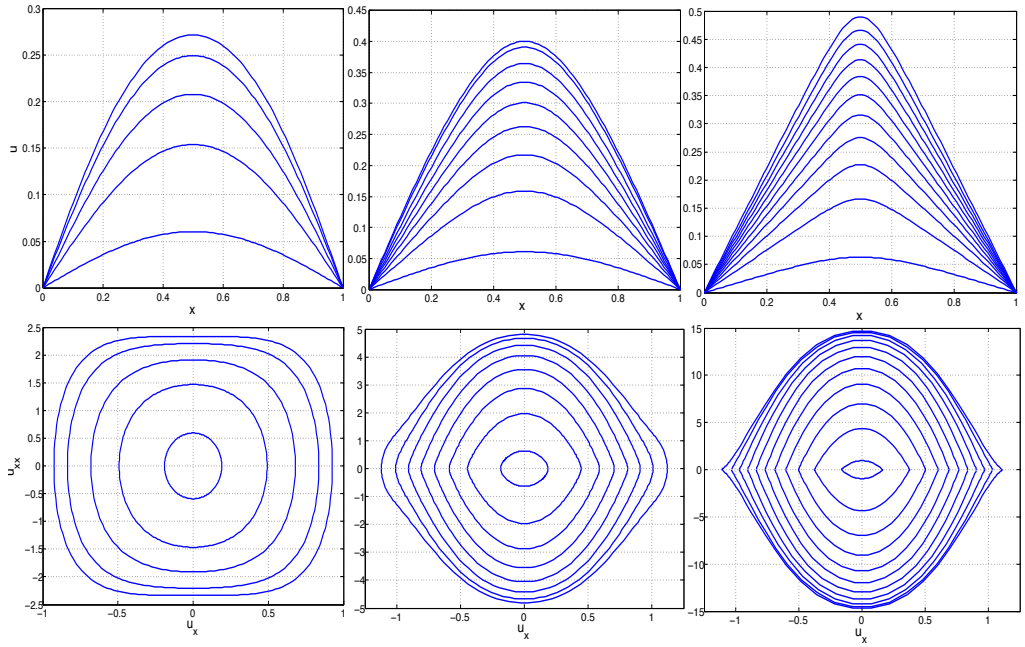

Figure 9: Solution profiles (x, u) (top row) and phase planes (u_x, u_{xx}) (bottom row) for $P^C < P < P_F$ (left) $k_2h^2 = 100$, (centre) $k_2h^2 = 1,000$, (right) $k_2h^2 = 10,000$. In each case $EI = k_1 = \ell/2 = 1$.

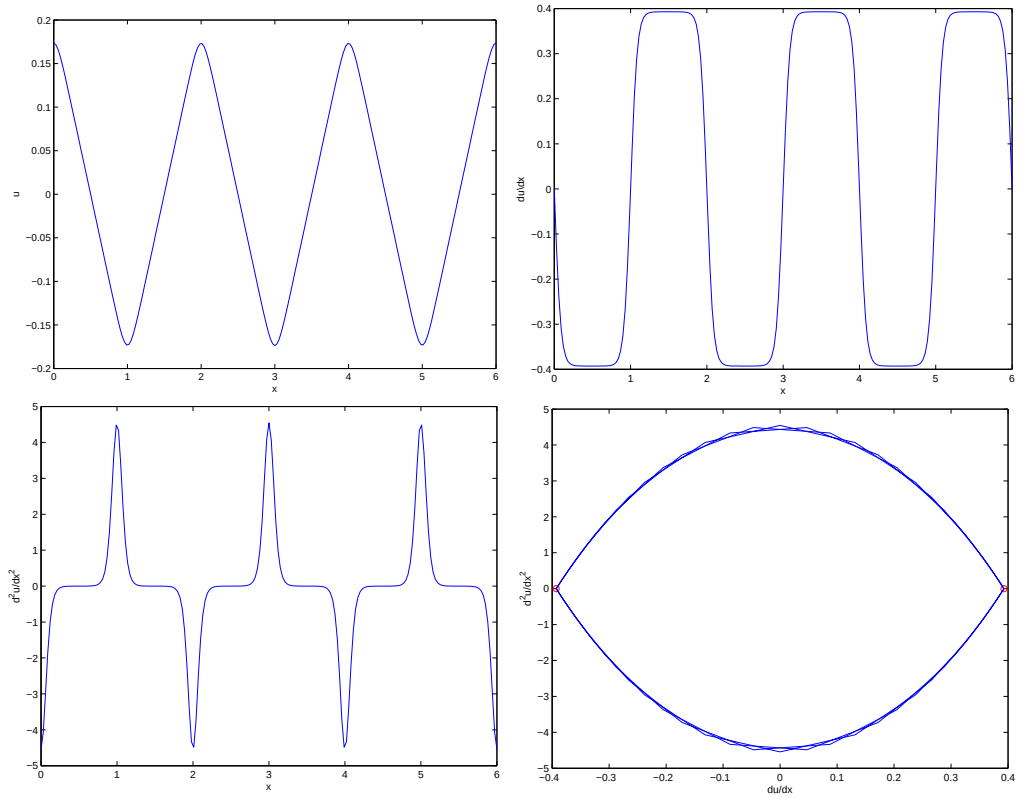

Figure 10: Solution profiles taken over 3 full periods. (top row) (x, u) (left) and (x, u') (right), for $P = 600$, $k_2h^2 = 10000$. In each case $EI = k_1 = \ell/2 = 1$. (bottom row) (x, u'') (left) and (u', u'') (right), for $P = 600$, $k_2h^2 = 10000$. In each case $EI = k_1 = \ell/2 = 1$.

Figure 11: Chevron folding at Millook Haven, Cornwall, UK. Note that the originally horizontal chevron folds have been tilted to near vertical by a later tectonic folding event. One of the author's lends scale to the picture.